EUROPEAN ORGANIZATION FOR NUCLEAR RESEARCH

CERN-EP/85-140
9 September 1985

A π^0 AND η SPECTROMETER OF LEAD GLASS AND BGO FOR MOMENTA UP TO 1 GeV/c

Basle[1]-Stockholm[2]-Thessaloniki[3] Collaboration

L. Adiels[2)], G. Backenstoss[1)], I. Bergström[2)], S. Carius[2)], S. Charalambous[3)], M.D. Cooper[1,4)], C. Findeisen[1)], D. Hatzifotiadou[3)], A. Kerek[2)], K. Papastefanou[3)], P. Pavlopoulos[1,*)], J. Repond[1)], L. Tauscher[1)], D. Tröster[1,*)], M.C.S. Williams[1,**)] and K. Zioutas[3)]

ABSTRACT

A spectrometer, consisting of two sets of bismuth germanium oxide (BGO) crystals and a lead-glass array, has been used to measure the π^0 and η momentum spectra produced from proton-antiproton annihilations at rest. We describe the tests of the BGO sets in an electron beam of energies from 50 to 450 MeV. We discuss the method of construction and calibration of the lead-glass array, as well as procedures to extract the energy and position resolutions for detected photons. A momentum resolution (σ) for π^0's and η's of 4% and 3%, respectively, has been achieved at momenta below 1 GeV/c.

(Submitted to Nuclear Instruments and Methods in Physics Research, A)

---

1) Institute of Physics, University of Basle, Switzerland.
2) Research Institute of Physics, Stockholm, Sweden.
3) Nuclear Physics Department, University of Thessaloniki, Greece.
4) Los Alamos National Laboratory, Los Alamos, N. Mex., USA.
*) Present address: CERN, Geneva, Switzerland.
**) Present address: University of California, Davis, Calif., USA.

1. INTRODUCTION

The detector that is described here has been designed for an experiment to search for exotic states in proton-antiproton annihilations [1] at the CERN Low-Energy Antiproton Ring (LEAR). For this purpose it was desirable to have the best possible momentum resolution and detection efficiency over the entire momentum range of decay products from $p\bar{p}$ annihilations at rest, i.e. up to 1 GeV/c.

The π^0 and η momentum spectra are obtained by measuring the two decay photons in coincidence (99% and 40% of all π^0 and η decays, respectively). The three observed quantities, the energies E_1 and E_2 of the photons, and the angle ϕ between them, determine the invariant mass m_0 of the two photons:

$$m_0^2 = 2E_1E_2(1 - \cos\phi). \tag{1}$$

Because the average number of π^0's produced in a $p\bar{p}$ annihilation is 1.9 [2], each resulting in two photons, there will be a substantial probability of finding a coincidence between photons from different π^0 mesons. These events yield a continuous background in the invariant mass spectrum. The π^0 and η momentum spectra are extracted by selecting events within a window centred at the mass of the π^0 or η, respectively.

The angle between the photons from a decaying π^0 or η is strongly correlated with the π^0 or η momentum through the Jacobian peak distribution. This distribution results from the transformation from the decay rest frame to the laboratory; it increases sharply towards a minimum decay angle ϕ_{min} given by

$$\phi_{min} = 2 \arctan (m/p) \ , \tag{2}$$

where m is the rest mass of the decaying particle and p is the magnitude of its momentum. There are three contributions to the invariant mass resolution:

$$(\sigma_m/m)^2 = (\sigma_{E1}/2E_1)^2 + (\sigma_{E2}/2E_2)^2 + [\sigma_\phi/2\tan(\phi/2)]^2 \ . \tag{3}$$

For small particle momenta, i.e. large angles ϕ, the last term of eq. (3) is negligible, even with poor angular resolution. The invariant mass resolution is then determined by the energy resolution. At higher momenta, the angular resolution term becomes important. Hence, good position resolution for the photon impact point on the detector and a small annihilation volume are crucial.

The highest π^0 momentum from $p\bar{p}$ annihilation at rest, 933 MeV/c, corresponds to a minimal photon angle ϕ of 16.5°, while zero momentum corresponds to $\phi = 180°$. In order to cover the whole momentum range, it is then necessary to span coincidence angles up to 180°. Although most decays occur close to the minimum angle, there is a substantial tail all the way out to 180°. Therefore, the acceptance of decay angles up to 180° also increases the efficiency for π^0's of higher momenta. At the minimum angle the decay is symmetric, i.e. $E_1 = E_2$, and occurs at a 90° centre-of-mass angle to the π^0 direction. The further away from the minimum angle the decay occurs, the bigger is the difference between the energies of the photons.

In principle, the π^0 and η momenta (p) are fully determined from the energies of the photons:

$$p^2 = (E_1 + E_2)^2 - m^2 \ , \tag{4}$$

where m is the true rest mass of the particle and **not** the measured invariant mass (m_0). By measuring the decay angle as well, we can improve the momentum resolution by kinematical fitting with an invariant mass constraint. The final momentum resolution then depends on the errors of the observables in an analogous way to eq. (3). To achieve good π^0 and η momentum resolution over the entire relevant momentum range, it is thus of interest to have both good photon energy resolution and good impact position resolution. To meet these requirements the detector was constructed from a large array of lead glass and two smaller BGO arrays. The lead glass has a large acceptance solid angle and good angular resolution, while the BGO sets provide excellent energy resolution.

The following section briefly describes the experimental set-up. In sections 3 and 4 we treat the performance of the BGO and lead-glass arrays as γ calorimeters. The combination of the detectors in a π^0/η spectrometer is then discussed in section 5. Finally the results are summarized in section 6.

2. BEAM AND DETECTOR ARRANGEMENT

Figures 1a and 1b show the experimental set-up. The two sets of BGO crystals are mounted on a ring surrounding the target. They can be moved to any azimuthal angle desired and are adjustable in the radial direction from 25 cm to 80 cm in order to be able to vary solid angle and angular resolution. The lead-glass array is rigidly installed below the beam line at a radius of 80 cm and subtends an angle of 120°, covering a total solid angle of 5.3%.

The experiment was performed in the C1 antiproton beam from the CERN LEAR machine. This antiproton beam of 200 MeV/c or 300 MeV/c momentum is completely free from contamination and has an intensity of between 10^4 and 10^5 $\bar{p}$ per second. As a result of the stochastic cooling [3] employed at LEAR, the longitudinal momentum spread $\Delta p/p$ of the beam is less than 10^{-3}.

Range straggling was measured at 300 MeV/c; a stop distribution of 8 mm FWHM in liquid hydrogen (LH_2) was obtained. Such a longitudinal uncertainty in annihilation position is unimportant for the angular resolution because the γ-ray detectors are placed in a plane normal to the beam. The beam diameter was measured just upstream of the target to be less than 5 mm FWHM. At 300 MeV/c beam momentum the mean range of the antiprotons was 11 cm of LH_2 after having passed through a 1 mm thick scintillator. Since multiple scattering introduces a negligible broadening of the beam diameter of less than 0.5 mm, the size of the annihilation volume is small enough to always contribute less to the angular resolution than the uncertainties in reconstruction of impact position on the detector.

3. THE BGO CALORIMETERS

The properties of BGO have been well documented elsewhere [4,5], and we recall only its main advantages here:

- a short radiation length of 1.12 cm, compared to 2.54 cm for NaI(T1)
- low afterglow (0.005% after 3 ms)
- good mechanical properties (non-hygroscopic).

The two sets of BGO crystals used in this experiment are identical in construction*). Each set consists of seven crystals with the shape of hexagonal prisms. These crystal elements are 20.3 cm long and 5.4 cm between parallel faces (see fig. 2). Each set is equipped with a hodoscope consisting of seven small BGO bars of dimensions $1.0 \times 1.2 \times 5.0$ cm^3. Figure 2 shows how these were placed in front of the hexagonal crystals. The BGO sets were placed at a distance of 30 cm from the target, covering a solid angle of 1.6% each. The BGO assemblies were housed in plastic boxes designed as a shield against rapid temperature variations in the experimental hall. Charged pions were recognized by plastic scintillators mounted in front of each set (see fig. 1a).

The BGO crystals were optically compensated to give a longitudinally uniform light output. The compensation was accomplished by partially wrapping them in optically diffuse paper. The crystals were also covered with 100 μm thick aluminum foil. The longitudinal non-uniformity of light output from such a crystal element has been measured with two methods. Firstly, a beam of 800 MeV/c (minimum ionizing) pions was used that traversed the crystal perpendicular to its symmetry axis at different distances from the front face. Secondly, a ^{137}Cs source illuminated the crystal through a 5 mm hole in a 5 cm thick lead collimator. The two methods gave consistent results: the non-uniformity of the crystals was found to be typically $\pm 2\%$ in the first 18 cm of their length. In fig. 3 we show the non-uniformity of the worst and the best crystal. The scintillation light is detected by Hamamatsu photomultiplier tubes (type R 1306-01)**) glued onto the rear surface of the crystals.

The energy resolution below 3 MeV has been investigated with γ-rays from the radioactive sources ^{203}Hg, ^{22}Na, ^{137}Cs, ^{88}Y, and ^{228}Th, which were attached to the front face of the crystal. The result, after subtracting the amplifier noise ($\sim$ 200 keV) quadratically, is shown in fig. 4a; the energy dependence can be fitted by the expression

$$\Gamma/E = 0.49\%/\sqrt{E}[\mathrm{GeV}] \ \text{(FWHM)} \ . \tag{5}$$

In this low-energy domain the resolution is mainly due to statistical fluctuations in the number of photoelectrons.

The calorimetric behaviour of our BGO sets was tested with electrons at energies from 50 to 450 MeV at the Schweizerische Institut für Nuklearforschung (SIN) cyclotron. The test was conducted at the πM3 beam, which has a momentum spread of less than 1%. Contaminating muons and pions were vetoed by a time-of-flight condition. The BGO set was placed with the beam along the symmetry axis of the central crystal. A 1×1 cm^2 trigger scintillator defined the impact position. The seven crystals of a set were intercalibrated using the signals from stopped muons and pions which, at a momentum of 300 MeV/c, deposit 212 MeV and 195 MeV, respectively.

By using electrons of varying energy, we checked the linearity of the BGO sets. The result is plotted in fig. 5. The deviation from a linear behaviour, expressed by the ratio ϵ/c after having

*) Manufactured by Harshaw Chemical Co., Solon, Ohio, USA.
**) Technical Data sheet No. PM-231-01, Hamamatsu TV Co., Hamamatsu, Japan.

fitted the second-order polynomial $E_{BGO}(E) = p + cE + \epsilon E^2$, amounts to $|\epsilon/c| = 10^{-5}$. We also determined the energy resolution as a function of the electron beam energy. The result is shown in fig. 4b; the energy dependence can be fitted by the expression

$$\Gamma/E = 2.65\%/\sqrt[4]{E}[\mathrm{GeV}] \ (\mathrm{FWHM}) \ . \tag{6}$$

At these higher energies the resolution is dominated by shower leakage outside the active detector volume. The curve included in fig. 4b is a Monte Carlo simulation using the SLAC-EGS program [6]. The agreement is good down to 100 MeV, but at 50 MeV EGS predicts a better resolution than measured. If we assume that the simulation includes all relevant effects, such as photon statistics and longitudinal non-uniformity, this discrepancy remains unexplained.

For reconstruction of the impact point one can use a simple centre-of-gravity algorithm:

$$x = \frac{\sum_{i=1}^{7} x_i E_i^{\alpha}}{\sum_{i=1}^{7} E_i^{\alpha}}, \qquad y = \frac{\sum_{i=1}^{7} y_i E_i^{\alpha}}{\sum_{i=1}^{7} E_i^{\alpha}}, \tag{7}$$

where (x_i, y_i) are the coordinates of crystal $i = 1, .., 7$ (see fig. 2). The free parameter α can be fixed by comparing the values of $|y|$ to data for which the impact position has been measured with the BGO hodoscope (see fig. 2). The best value was found to be $\alpha = 0.375$.

Because the formulae (7) are based on the shower spread, the accuracy of the position (x,y) will clearly be dependent on the shower energy. This centre-of-gravity method works well for higher photon energies, yielding a position resolution r.m.s. of 0.55 cm at a photon energy of 428 MeV. At lower energies the shower spread is not as large and fluctuations are more dramatic, reducing the utility of the centre-of-gravity method. Knowing the energy resolution as a function of energy [eqs. (5), (6)], we adopt a heuristic formula for the resolution of the position calculated with eq. (7) as a function of the shower energy: $\sigma_x = 0.5 \text{ cm} \cdot E^{-\beta}$, where E is in GeV and β is a free parameter. The value $\beta = 1/2.7$ fitted the observed angular resolution values (cf. Section 5). As discussed earlier, the asymmetric π^0 and η decays give photons with low energy, and thus one of the two first terms of eq. (3) is large. To improve the π^0 or η momentum resolution we depend on good angular resolution for photons with lower energy. For this reason we equipped each BGO set with a hodoscope as described earlier. The position resolution obtained with these hodoscopes is independent of the photon energy and is given by the standard deviation $1.0 \text{ cm}/\sqrt{12} = 0.29 \text{ cm}$.

Photons striking a BGO result in two types of events. For those photons that convert in the hodoscope (54%), the geometry of the hodoscope produces a well-defined solid angle of 0.3%, because the BGO hexagons have enough lateral extent to contain such showers entirely. For the photons that do not convert in the hodoscope (46%), the effective solid angle is determined by conditions on the deposited energy, applied in the off-line analysis. Firstly, it is required that accepted events contain more than 15% of the total energy (E_{tot}) in the central crystal. Additionally, if a peripheral crystal registers the maximum energy (E_{max}), the central crystal must still have the majority of the remaining energy $E_{tot} - E_{max}$. These cuts make the effective solid angle approximately 0.5%. Using the hodoscope has the drawback of decreasing the trigger rate by roughly a factor of 2 due to conversion inefficiency and of deteriorating the energy resolution of the system.

Passing charged pions have been continuously monitored throughout the experimental run. The corresponding events are defined by simultaneous signals from the plastic scintillators in front of and behind the BGO set (see fig. 1a) and energy deposited in the BGO. Only those events where a single BGO crystal contains energy are selected in an off-line analysis. The energy released by these pions gives a peak at 198 MeV in the spectrum from a BGO hexagon (see fig. 6). These peaks were used for intercalibration and correction of the intercalibration drifts. For a LEAR run period, which typically extends over a few days, the intercalibration uncertainty was less than 0.5% (mainly due to drifts). We also used the inclusive γ-spectra from each individual crystal for intercalibration by fitting a square root expression to the high-energy part of the spectra, and by adjusting the end points to be 933 MeV. This method was consistent with the one using charged pions.

4. THE LEAD-GLASS ARRAY

The lead-glass array consists of 160 elements that are fabricated from type F2 glass*) that has a radiation length of 3.05 cm, a density of 3.61 g/cm^3, and a refractive index of 1.62. The wedge-shaped blocks are 50 cm long with front faces of 4.2 $\times$ 6.4 cm^2 and rear faces of 6.4 $\times$ 6.4 cm^2 (see fig. 7). The blocks are stacked in four rows of 40 blocks transverse to the beam, and they extend 25.6 cm in the direction of the beam. The distance from the target centre to the front face of each block is 80 cm. A double layer of 80 plastic scintillators, each covering 8 lead-glass blocks, is used to veto charged pions. In the off-line analysis only those photons are accepted that hit the lead-glass array at $|z| < 9$ cm (see fig. 1); this results in an effective solid angle of approximately 3.7%.

Each lead-glass block is wrapped in 20 μm thick aluminized mylar foil and is covered with black PVC foil. The two-inch EMI-9839B photomultiplier (PM) covers 1/3 of the area of the rear face; it is glued onto the surface with Epotek 301-2 (this epoxy has a refractive index of 1.54)**). The signals from the PMs are sent to the counting room, where they are split threefold. One part of each signal is sent via a 160 ns delay cable to a LeCroy 4300 FERA ADC. These ADCs have a conversion time of about 10 μs and are used in the sparse-readout, pedestal-subtraction mode. Data are read out via the LeCroy ECL bus at a rate of 100 ns per word. The other parts of each split signal are fed to the fast trigger electronics that determines the number of clusters and where the energy is deposited in the array.

In order to monitor the gain of the individual PMs, each lead-glass block is equipped with an ^{241}Am α-source mounted on a small piece ($\varnothing$ 8 $\times$ 2 mm^3) of plastic scintillator. The scintillator is glued to the rear end of the block close to the PM. The light pulse produced is equivalent to a shower of between 20 and 60 MeV; variations occur from block to block owing to differences in light coupling of source scintillator.

The preliminary relative calibration of the elements in the array is performed by using cosmic rays. Only events with energy in a single block are selected in this procedure. The deposited energy, in this case, is equivalent, on the average, to a 500 MeV shower. Depending on the orientation of the block, it takes between 12 and 48 hours to accumulate a peak with 60 counts. This method is limited by statistics; relative matching of the order of 10% is achieved this way. A secondary method employed a data sample obtained during an experimental run. A loose

*) Manufactured by Jenaer Glaswerk Schott & Gen, Mainz, FRG.
**) Epotecny, Vélizy, France.

trigger condition is used so that the array is uniformly illuminated with γ-rays. This trigger consists of an incoming antiproton and more than 10 MeV energy deposit in the lead glass. For each block an exponential is fitted to the measured spectra, and intercalibration constants are derived by equalizing the exponents. By this method an intercalibration of better than 5% is achieved.

During off-line analysis, we use the π^0 and η data itself to further adjust the calibration by creating an invariant mass plot for each block. The events selected are restricted to those with two (or more) photons in the lead-glass array and those with at least 60% of the cluster energy in the element being plotted. Figure 8 shows the position of the π^0 invariant mass peak for each of the 160 blocks. The bottom view in fig. 8 is the projection onto the mass axis, which reveals a FWHM of 6% for the distribution. Because

$$(\delta E/E) = 2\,(\delta m_0/m_0)\ , \tag{8}$$

the calibration constants are derived easily. Repetition of this procedure for different runs shows that the constants for each block change by a few per cent per hour. Because these drifts do not contribute significantly to the energy resolution of the array in the energy range of interest, no corrective measures were undertaken.

Figure 9a shows the position of the π^0 invariant mass peak as a function of the energy E_1 of one photon, while the energy E_2 of the other photon is kept "constant". In practice, in order to achieve enough statistics, E_2 is selected to be between 200 and 300 MeV. The observed function reveals a non-linear energy dependence, which can be corrected by using the following expression (E_γ in MeV):

$$E'_\gamma = E_\gamma - 0.00004E_\gamma^2 + 2\ . \tag{9}$$

The corrected spectrum is shown in fig. 9b.

In fig. 10 we show the average number of blocks involved in a shower as a function of the shower energy. Below 100 MeV a position algorithm such as the centre-of-gravity method described earlier, can do no better than the width of a block. A more refined position algorithm was constructed to give a flat distribution as the response to the loose trigger run discussed previously, during which the lead-glass array was uniformly illuminated with photons. This algorithm consists firstly of calculating the position from the energy-sharing between neighbouring blocks and secondly of a mapping (using a look-up table) in order to correct for finite intercalibration and shower leakage from the edge blocks. We checked the accuracy of this algorithm by inspecting the opening angle spectrum from η decays. In this spectrum there is a Jacobian peak originating from the reaction

$$p\bar{p} \rightarrow \eta + \omega$$

that gives monoenergetic η's with 656 MeV/c momentum. The two photons from the decay occur at a minimum angle of 79.8°. The observed spectrum is shown in fig. 11. From a fit we deduce the position resolution at 428 MeV to be 1.4 cm (FWHM), i.e. a standard deviation of 0.59 cm. For the further evaluation we assume that the position resolution varies as one over the square

root of the energy in GeV, and that it can never be worse than the width of a block, i.e. a standard deviation of 4.2 cm/$\sqrt{12}$ = 1.2 cm (cf. section 3).

By inferring an angular resolution from this position resolution, we can perform a Monte Carlo simulation of the expected width of the π^0 invariant mass peak as a function of the π^0 momentum. Because the energy resolution is governed by photon statistics, we employ a resolution function characterized by

$$\Gamma/E = x\%/\sqrt{E}[\text{GeV}] \text{ (FWHM)} \tag{10}$$

In this expression x is the resolution parameter to be determined. In fig. 12 we show three curves fitted to the Monte Carlo results for three different values of x respectively, namely 6%, 7%, and 8%. A comparison with the experimental data points demonstrates that x is slightly larger than 7%. It should be emphasized that the data points from lower-momentum π^0's are most sensitive to the energy resolution.

5. PERFORMANCE OF THE π^0/η SPECTROMETER

The movable BGO arrays are arranged to optimize for π^0's and η's with different momenta. By combining detector signals, we create four principal coincidence configurations:

i) One photon detected by a BGO set and the other photon detected by the other BGO set (BB coincidence).
ii) One photon detected by a BGO set and the other photon detected by the lead-glass array, where the angle between the BGO and the lead glass is big enough so that 180° coincidence angles are included (BL_1 coincidence).
iii) Same as case (ii), but with the BGO placed as close as possible to the lead glass so that the diametrically opposite point of the BGO falls outside the lead glass (BL_2 coincidence).
iv) Both photons detected by the lead-glass array (LL coincidence).

These four detector configurations cover different momentum ranges, where by 'range' we mean the momentum intervals for which the minimum decay angle is subtended by the detectors [cf. eq. (2)]. Higher energy π^0's outside the actual range can, however, be detected with lower efficiency because the decay-angle distribution has a tail extending to 180°. The momentum ranges covered by the three last configurations are listed in table 1. Cuts in the off-line analysis diminish the azimuthal angle accepted by the lead glass by roughly half a block at each end of the array. Thus, the ranges in table 1 are calculated assuming the effective azimuthal angle subtended by the lead glass is from $-58.5°$ to $+58.5°$. The combination BB is uninteresting because its range is very small.

A sample of π^0's (or η's) decay uniformly in the centre-of-mass system, but are characterized by eq. (1) in the **laboratory**. Thus, the laboratory acceptance for a particular momentum cannot be derived from the solid angles of the detectors in a simple way. The acceptance curves in figs. 13a to 13c have been calculated using Monte Carlo techniques, and show the acceptance of π^0's and η's for the three detector combinations BL_1, BL_2, and LL, respectively. The vertical axis is the percentage of π^0's or η's accepted relative to the number produced in the target. The branching ratio BR($\eta \rightarrow 2\gamma$) = 0.4 is **not** included in this acceptance. For the detector combinations BL_2 and LL the acceptance rises quite linearly from a minimum momentum,

whereas for BL_1 it falls off very rapidly from momentum zero. The small 'kink' on the π^0 acceptance curve around 90 MeV/c is due to the π^0's going out of range.

The π^0 and η momentum spectra are extracted by a least squares fit of the kinematics. To perform this procedure, the errors used in weighting the measurements must be determined. The errors in the energies have been discussed in previous sections. The angular resolution, however, needs further comment. The angular resolution is determined from the uncertainty in defining the directions of the two photons. The direction is given by the emission point and the impact point on the detector. The π^0 source is the annihilation region that has an r.m.s. width of 0.21 cm. For a photon converting in the BGO hodoscope, the position resolution distribution has a standard deviation of 0.29 cm. For a photon that converts in the hexagons, the centre-of-gravity algorithm is used to obtain the impact point, yielding a position resolution distribution with a standard deviation of about 0.7 cm. This is dependent on the energy deposited (see section 3). The position algorithm for the lead glass gives a distribution for the impact position with a standard deviation of about 0.6 cm (also energy dependent). The widths of the distributions for the angular resolutions are derived by folding the contributions from the emission point and the impact points to yield a standard deviation of 0.68° for hodoscope conversions, 1.4° for hexagon conversions, and 0.46° for lead-glass conversions.

Figures 14a to 14c show the invariant mass spectra for the three detector combinations BL_1, BL_2, and LL, respectively; the inset in fig. 14c is a magnification of the tail. There are two peaks in the invariant mass spectra, one from π^0's, the other from η's. The first cut applied in the evaluation of the data is to restrict the invariant mass to be within three standard deviations from the π^0 or η mass. The remaining data sample after this cut was processed by a 1C kinematical fitting program [7] that used the invariant mass equation (1) with m_0 equal the rest mass of the particle as a constraint. This improves the π^0 momentum resolution by as much as a factor of 3 for LL events, relative to just summing the two photon energies. The χ^2-values obtained from the fit are in agreement with the theoretical curve for one degree of freedom up to a value of $\chi^2 = 3.8$, corresponding to a 95% confidence level. For the LL coincidences in the π^0 window a χ^2-cut at this value reduced the data sample by 25%. The peak-to-background ratio in this window is 1.04, implying that 91% of the events thrown away are uncorrelated coincidences, or, equivalently, 46% of the uncorrelated background is rejected. This result is confirmed by a Monte Carlo simulation. The method should be compared to simply making a cut in the invariant mass spectrum: to get 95% confidence level this cut has to be applied at ± 2 standard deviations. This only affects 10% of the data sample, i.e. hardly 17% of the uncorrelated coincidences are removed.

6. RESULTS AND SUMMARY

The data sample remaining after the χ^2-cut is then used to produce the final momentum plots, shown in figs. 15 and 16. The peaks around 770 MeV/c in the BL_2 and LL spectra stem from the two-body decays $p\bar{p} \rightarrow \pi^0\varrho^0$ and $p\bar{p} \rightarrow \pi^0\omega$, whereas the peak in the LL η spectrum (fig. 16) arises from the reactions $p\bar{p} \rightarrow \eta\varrho^0$ and $p\bar{p} \rightarrow \eta\omega$. By assuming the errors according to sections 3–5, the π^0 and η momentum resolutions versus momentum can also be obtained by a Monte Carlo simulation. The results are shown in fig. 17. The momentum resolution can be checked against data for the following two cases. Firstly, the π^0 momentum resolution can be measured at 768 MeV/c where there is the peak from π^0's recoiling from a ϱ^0 or ω meson. Taking the intrinsic width of the ϱ^0 into account (80 MeV/c in this spectrum), the measured r.m.s. width

is 3.8% for LL in agreement with the Monte Carlo curve in fig. 17. The other case is the corresponding peak in the LL η momentum spectrum from η's recoiling from a ϱ^0 or ω meson. The r.m.s. width of this peak at an η momentum of 656 MeV/c is 2.9%, also agreeing well with the Monte Carlo results.

Finally, we summarize the observed performance of the detectors. We have tested a modular BGO calorimeter in an electron beam of 50 to 450 MeV and have used it for detecting photons up to 1 GeV. We obtain the following results:

- an energy resolution of about 3% FWHM at 1 GeV, which is consistent with expectations,
- a spatial resolution of about 1.3 cm FWHM for reconstruction of impact position from shower topology,
- an intercalibration and a drift correction that are better than 1% with a method employing through-going charged pions.

We have used a large, modular lead-glass detector to measure photon–photon coincidence events. From the data analysis we observe the following:

- the energy resolution is $7\%/\sqrt{E}$ [GeV];
- the spatial resolution for impact position reconstruction from shower topology is about 1.4 cm FWHM;
- the intercalibration and drift correction can be made better than 5% by using the π^0 invariant mass peaks.

When the two calorimeters are used as a π^0 and η spectrometer, they yield:

- a momentum resolution with a standard deviation of 3.8% for 768 MeV/c π^0's and with a standard deviation of 2.9% for 656 MeV/c η's;
- good momentum acceptance from 0–1 GeV/c;
- feasible solid angles for high-statistics spectroscopy at LEAR.

Acknowledgments

This work was supported by the Swiss National Science Foundation, the Swedish Research Council, and the Greek Administration for Research & Technology. We also wish to thank CERN for support and hospitality. Our special thanks go to: Å. Engström (Stockholm), K. Agehed (Stockholm), and H. Krause (Basle) for mechanical-engineering support and to H.O. Meyer (Indiana) for his contributions in preparing this publication.

REFERENCES

[1] L. Adiels, G. Backenstoss, I Bergström, K. Fransson, A. Kerek, P. Pavlopoulos, J. Repond, L. Tauscher, D. Tröster, K. Zioutas, Basle-Stockholm-Thessaloniki Collaboration, Proposal CERN/PSCC/80-142, PSCC/P 36 (1981).

[2] C. Ghesquière, CERN 74-18 (1974), p. 436.

[3] D. Möhl, G. Petrucci, L. Thorndahl, S. van der Meer, Phys. Rep. 58 (1980) 73.

[4] P. Pavlopoulos, G. Backenstoss, M. Hasinoff, J. Repond, L. Tauscher, D. Tröster, M. Rousseau, K. Fransson, G. Alberis, K. Zioutas, Nucl. Instrum. Methods 197 (1982) 331.

[5] H. Dietl et al., Performance of a BGO calorimeter with photodiode readout and with photomultiplier readout at energies up to 10 GeV, Max Planck Institute Munich Preprint MPJ/PAE/Exp. E1. 124.

[6] R.L. Ford and W.R. Nelson, Internal Report SLAC-210 (1978).

[7] B. Ronne, CERN 64-13 (1964), p. 87.

Table 1: Momentum ranges

Detector combination	BGO angle (ϕ) in fig. 1a (°)	π^0 momentum range (MeV/c)	η momentum range (MeV/c)
BL_1	185	0–84	0–340
BL_2	85	45–570	180–2300
LL		83–1300	340–5200

Figure captions

Fig. 1 The experimental set-up: a) cross-section perpendicular to the beam, b) vertical cross-section through the beam axis; the lead-glass and BGO detectors are shown as well as the corresponding charged-particle veto scintillators VL and VB. The scintillators SP are used to tag passing pions. The incoming antiproton beam is moderated in M and tagged by scintillator T.

Fig. 2 BGO assembly; also shown is the front hodoscope (H).

Fig. 3 Longitudinal non-uniformity in light output as a function of the distance d from the photomultiplier. Data for the most- and the least-uniform crystals are shown as open and closed symbols, respectively.

Fig. 4 Energy resolution of a BGO set. a) The low, and b) the high-energy performance are shown.

Fig. 5 Measurement of the response, E_{BGO}, of the BGO assembly using monochromatic electrons.

Fig. 6 The spectrum obtained from charged pions passing through one of the hexagonal BGO crystals in the longitudinal direction.

Fig. 7 View and dimensions of one of the elements of the lead-glass array.

Fig. 8 Position of the π^0 invariant mass peak for the 160 individual lead-glass blocks. The projection onto the mass axis is also shown.

Fig. 9 Position of the π^0 invariant mass peak versus the energy of one decay photon. The energy of the other photon is kept between 200 and 300 MeV/c: a) before any corrections, and b) after correcting for non-linearities.

Fig. 10 Number of lead-glass blocks involved in a γ shower versus shower energy.

Fig. 11 Observed distribution of the angle between the decay photons from the process $\eta \to \gamma\gamma$, where both photons are detected by the lead-glass array: a) the full range of angles; b) a fit to the peak resulting from the processes $p\bar{p} \to \eta\varrho^0$ and $p\bar{p} \to \eta\omega$ for a subset of the data on an expanded scale. Γ is the extracted angular resolution.

Fig. 12 Resolution of the π^0 invariant mass peak versus π^0 momentum for LL data. Measured values are compared with Monte Carlo predictions for three different lead-glass energy resolutions (curves, see text).

Fig. 13 Acceptance of three detector combinations for π^0 and η mesons obtained from Monte Carlo simulations.
a) BL_1: the BGO is placed opposite to the lead glass.
b) BL_2: the BGO is placed close to the lead glass.
c) LL: both photons are within the lead glass.

Fig. 14 Invariant mass spectra from the three detector combinations: a) BL_1, b) BL_2, c) LL.

Fig. 15 π^0 momentum spectra measured with the three detector combinations: a)BL_1, b) BL_2, c) LL.

Fig. 16 η momentum spectrum obtained from LL coincidences.

Fig. 17 π^0 and η momentum resolution plotted against momentum predicted by a Monte Carlo simulation.

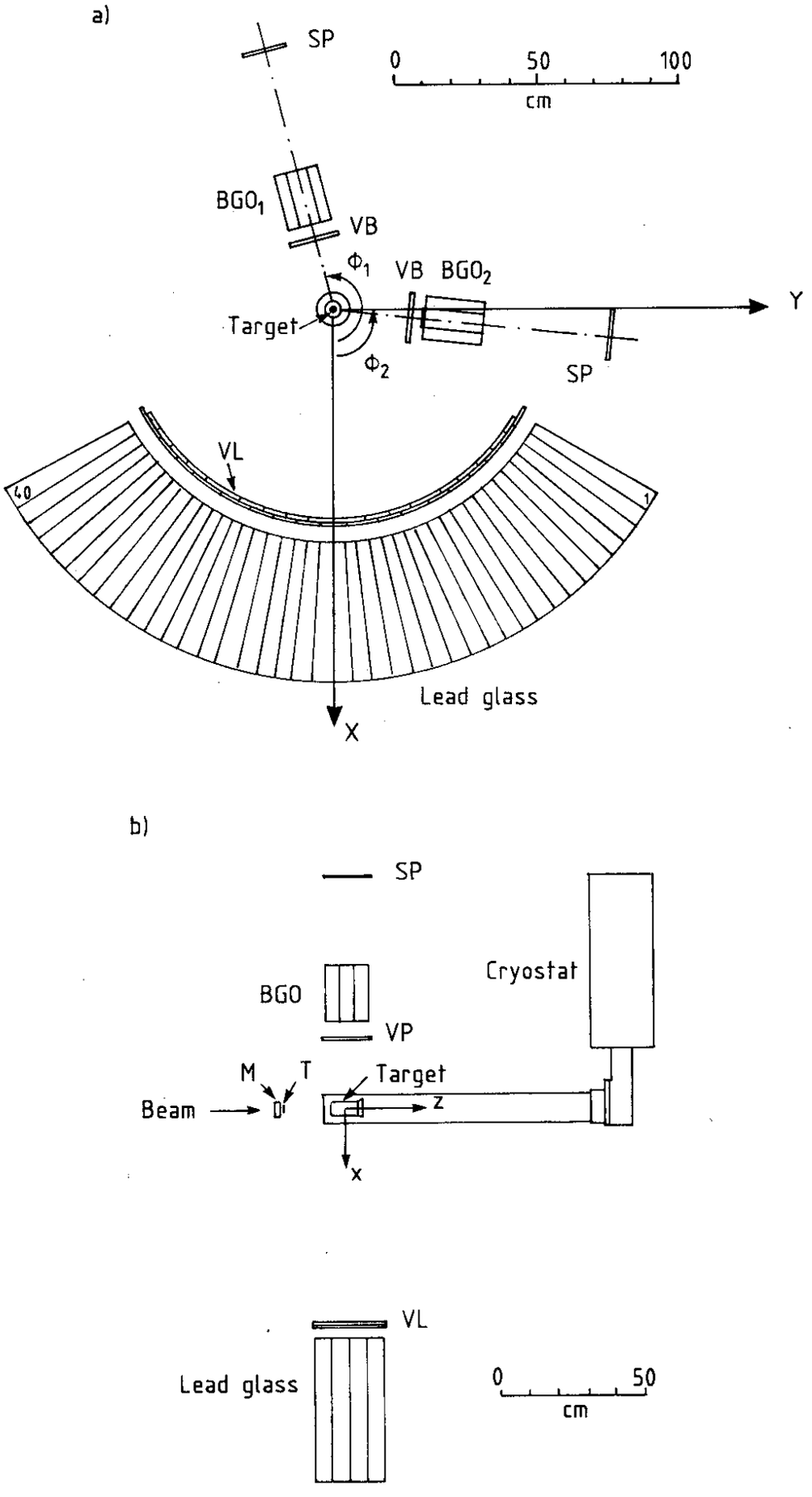
a)
SP
0
50
100
cm
BGO1
VB
Φ1
VB
BGO2
Y
Target
Φ2
SP
VL
40
1
Lead glass
X
b)
SP
Cryostat
BGO
VP
M
T
Target
Beam
z
x
VL
Lead glass
0
50
cm

Fig. 1

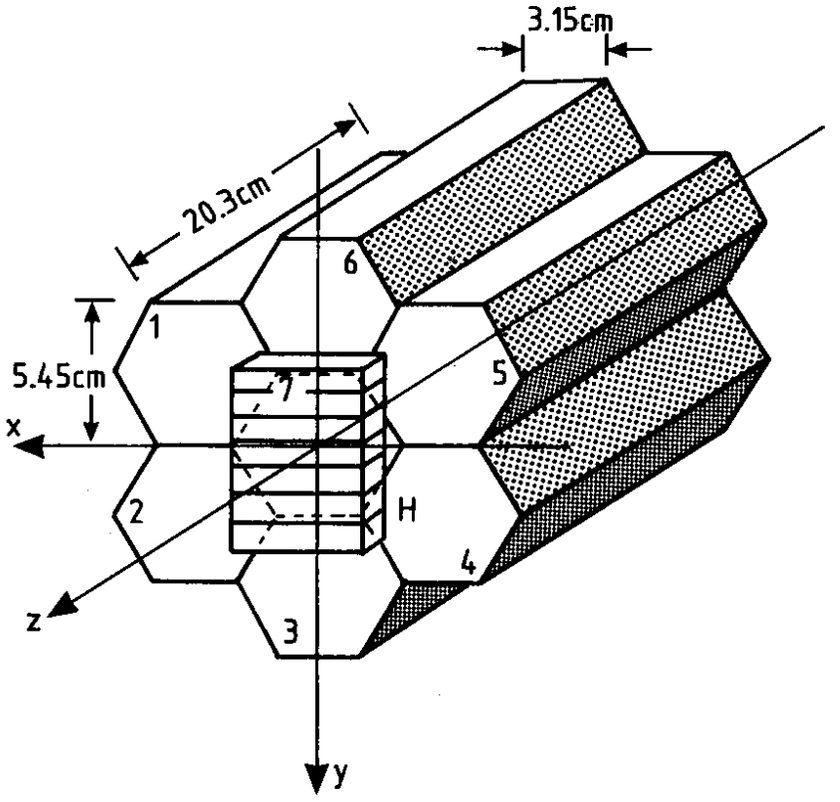
3.15cm
20.3cm
5.45cm
x
z
y
1
2
3
4
5
6
7
H

Fig. 2

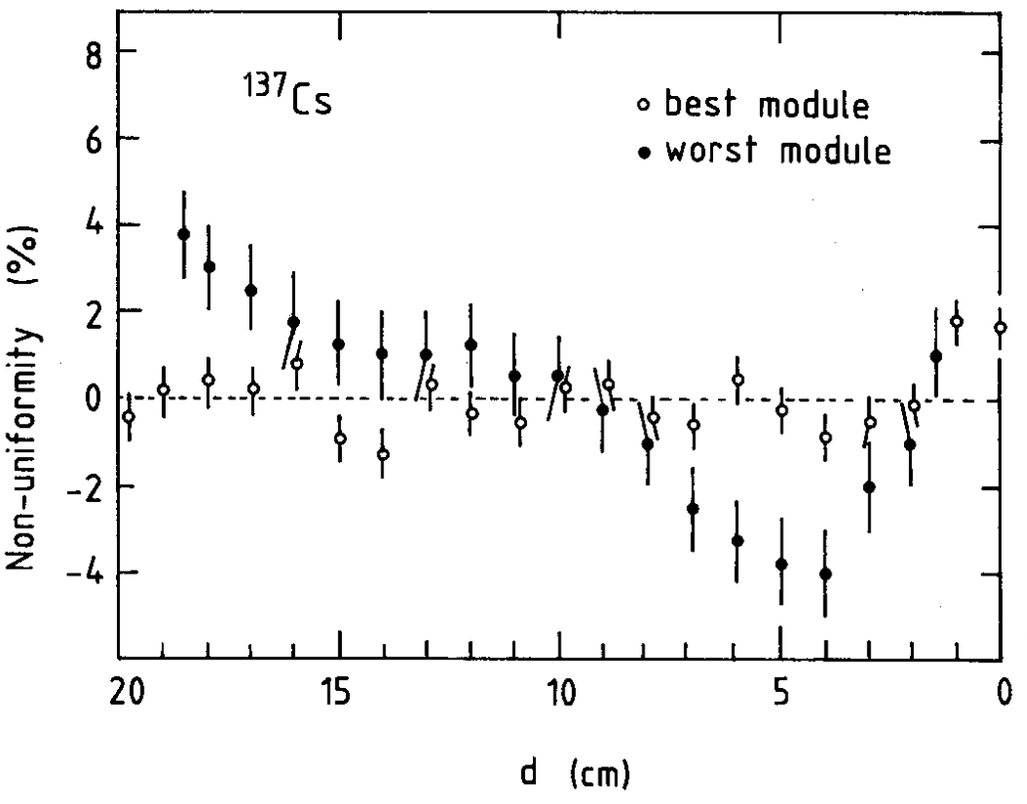
^{137}Cs
o best module
• worst module
Non-uniformity (%)
8
6
4
2
0
-2
-4
20
15
10
5
0
d (cm)

Fig. 3

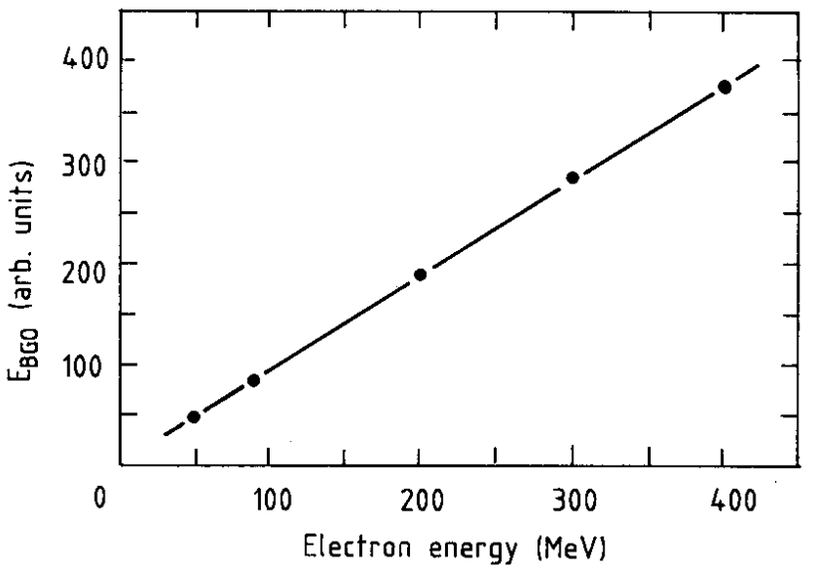

Fig. 5

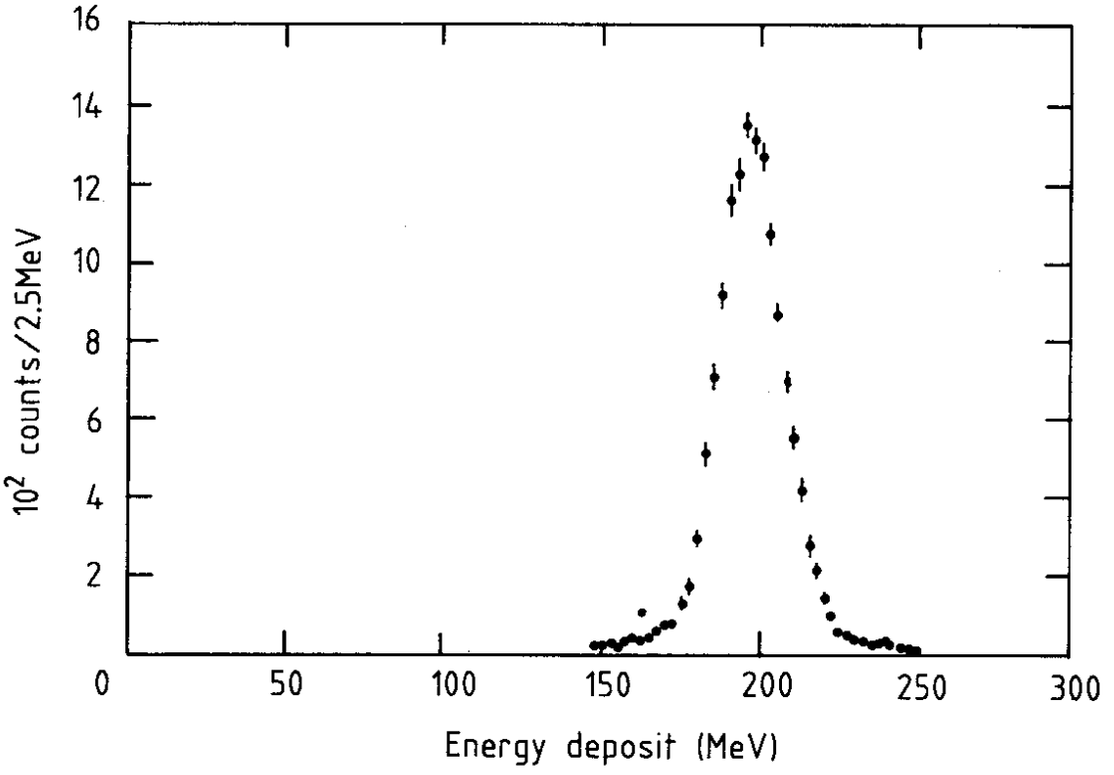

Fig. 6

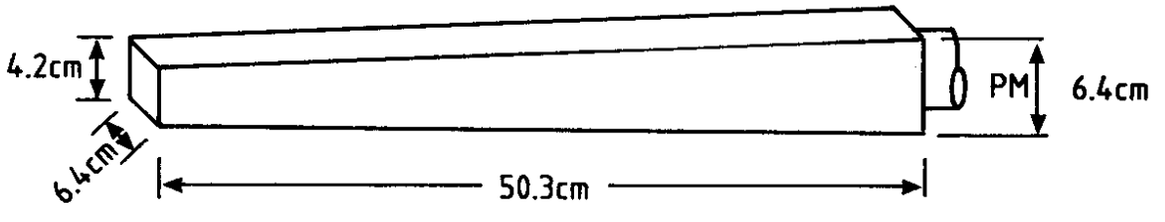

Fig. 7

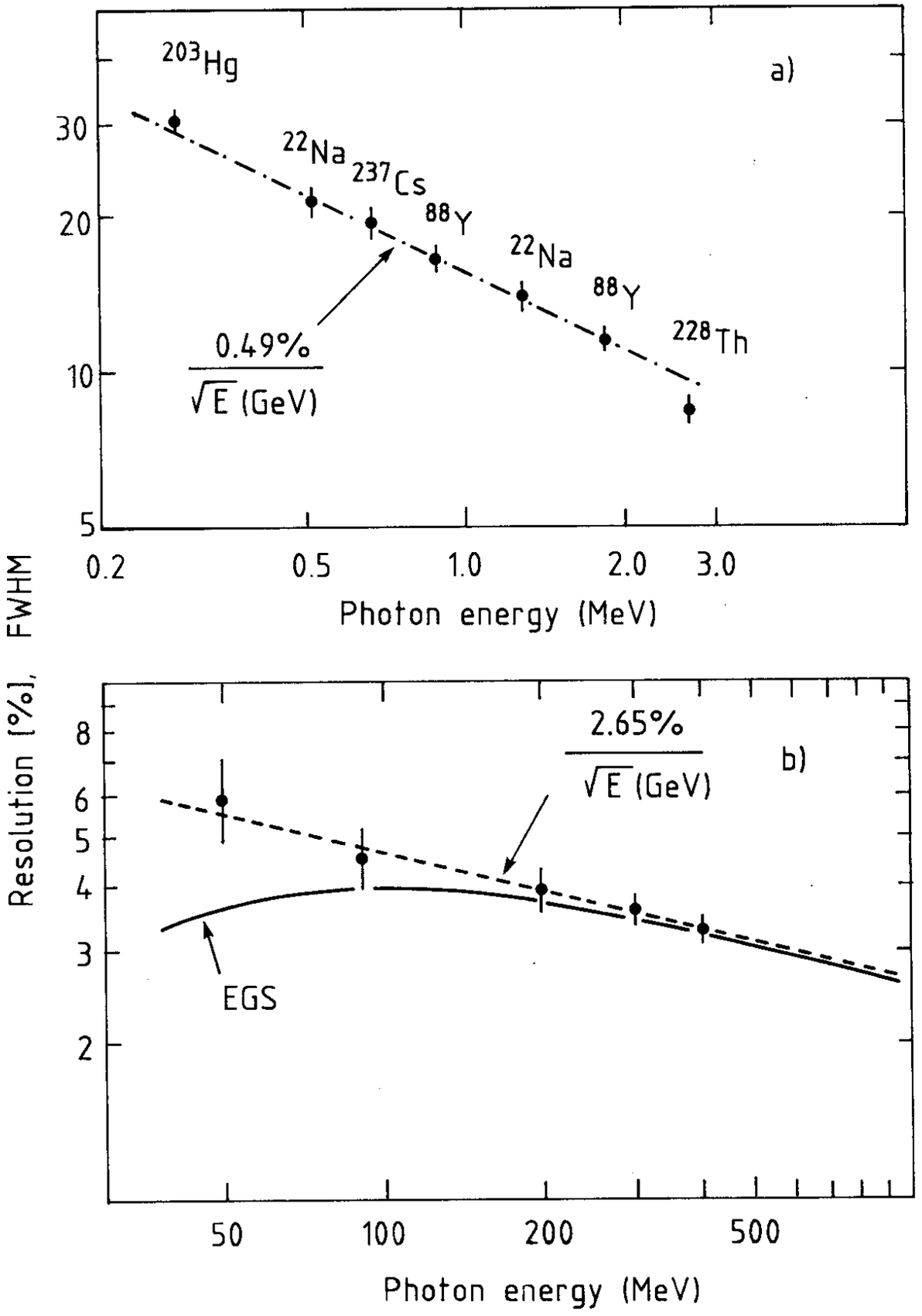
a)
^{203}Hg
^{22}Na
^{237}Cs
^{88}Y
^{22}Na
^{88}Y
^{228}Th
0.49%
√E (GeV)
30
20
10
5
0.2
0.5
1.0
2.0
3.0
Photon energy (MeV)
Resolution [%], FWHM
b)
2.65%
√E (GeV)
EGS
8
6
5
4
3
2
50
100
200
500
Photon energy (MeV)

Fig. 4

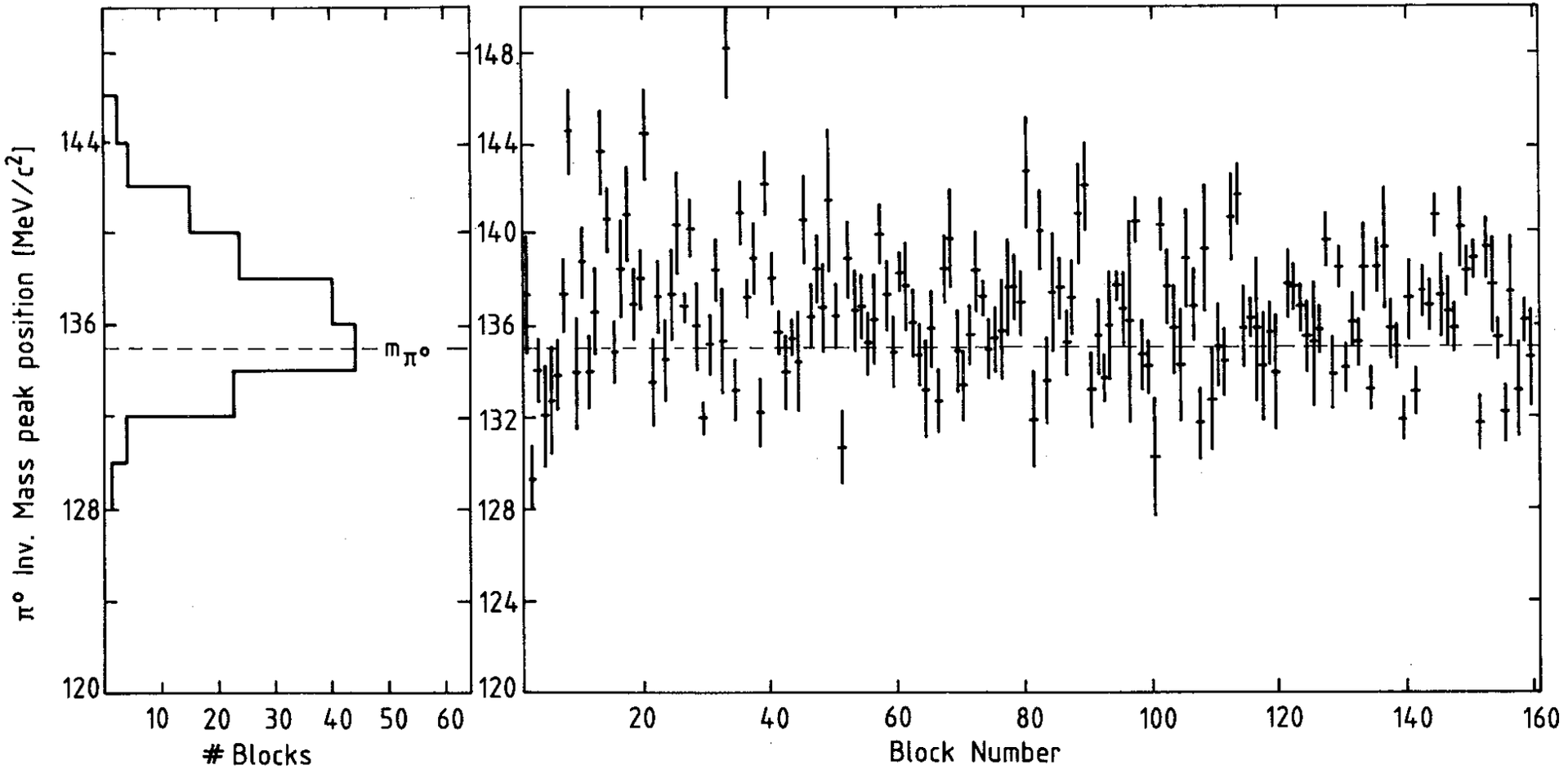
π° Inv. Mass peak position [MeV/c²]
144
136
128
120
m_{π°
10
20
30
40
50
60
Blocks
148
144
140
136
132
128
124
120
20
40
60
80
100
120
140
160
Block Number

Fig. 8

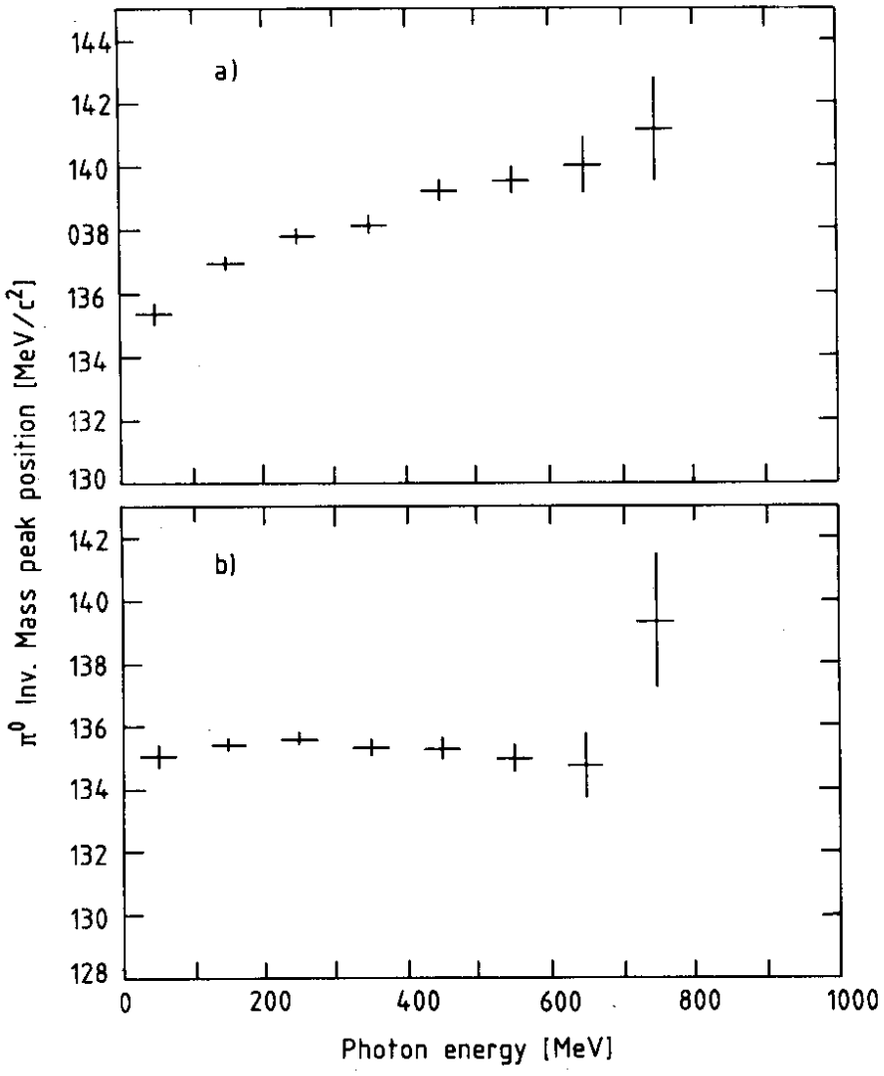
a)
b)
144
142
140
038
136
134
132
130
142
140
138
136
134
132
130
128
0
200
400
600
800
1000
π^0 Inv. Mass peak position [MeV/c^2]
Photon energy [MeV]

Fig. 9

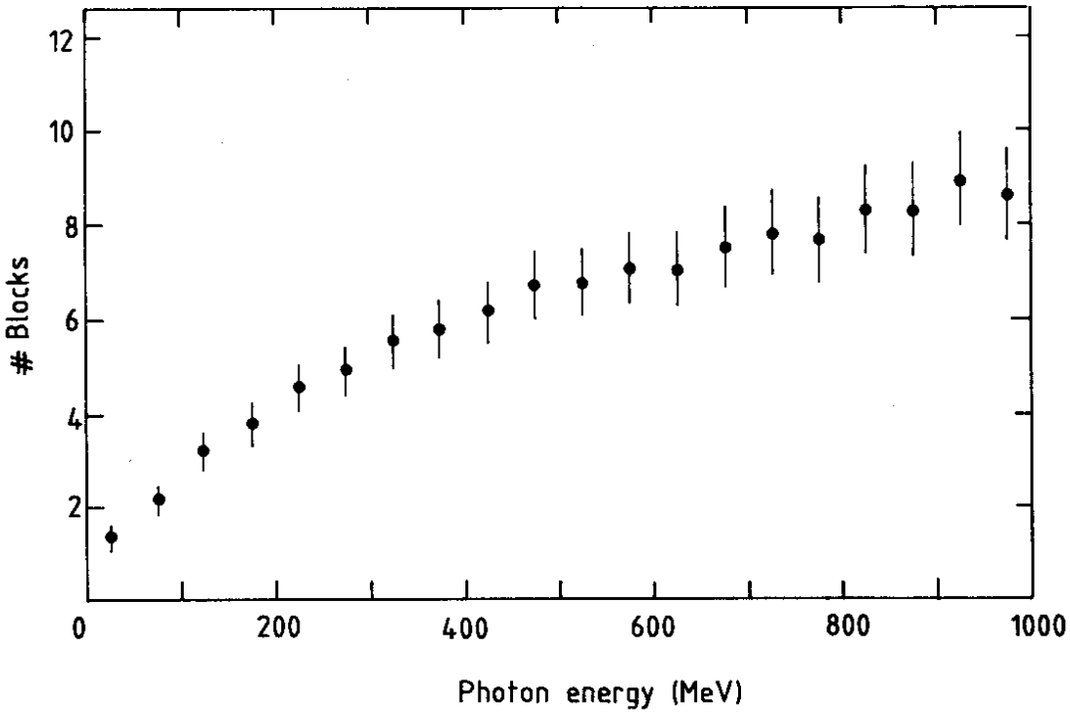
12
10
8
6
4
2
0
200
400
600
800
1000
Blocks
Photon energy (MeV)

Fig. 10

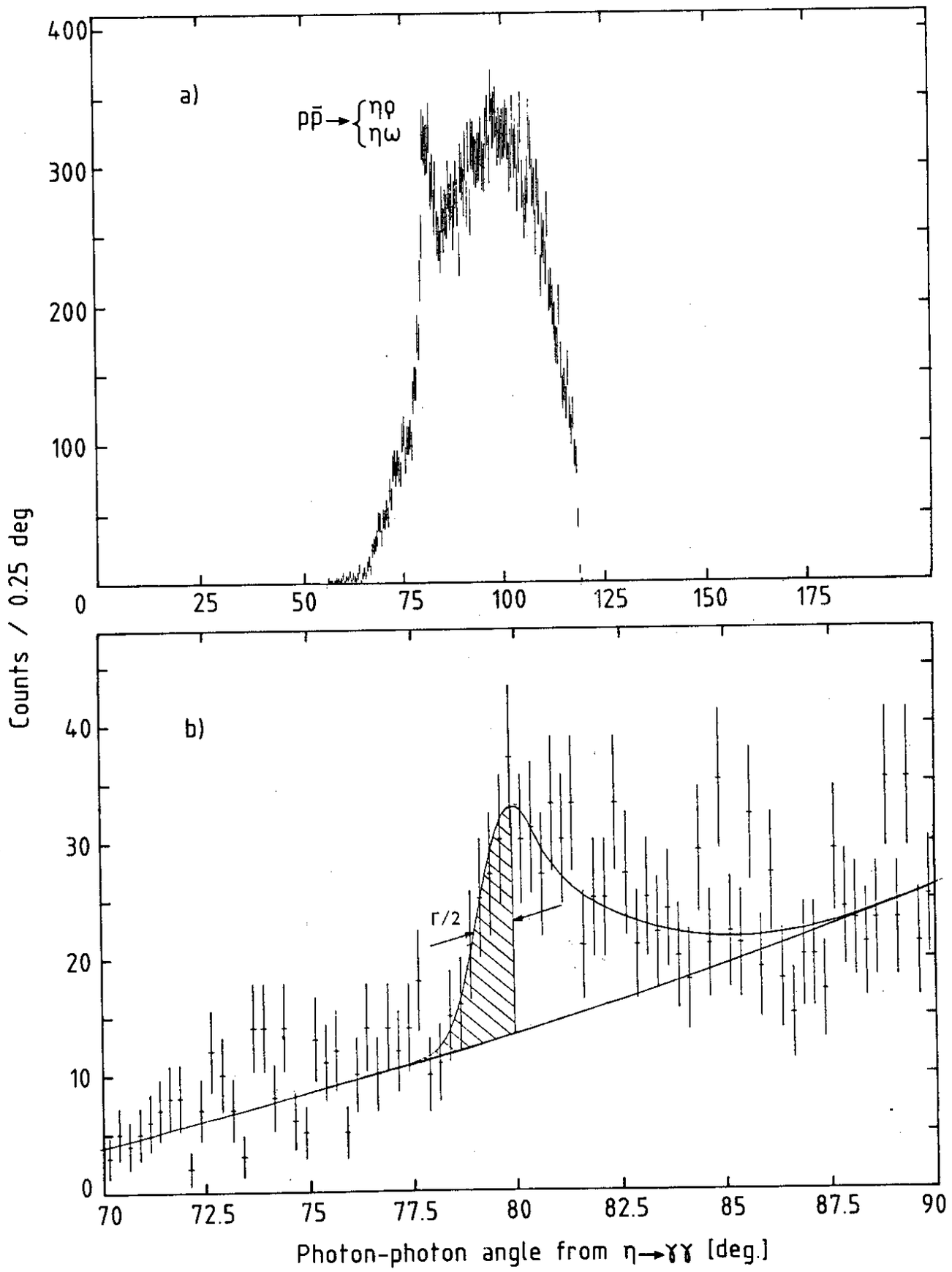
a)
$p\bar{p} \rightarrow \begin{cases} \eta\varphi \\ \eta\omega \end{cases}$
400
300
200
100
0
25
50
75
100
125
150
175
b)
40
30
20
10
0
70
72.5
75
77.5
80
82.5
85
87.5
90
Γ/2
Counts / 0.25 deg
Photon-photon angle from $\eta \rightarrow \gamma\gamma$ [deg.]

Fig. 11

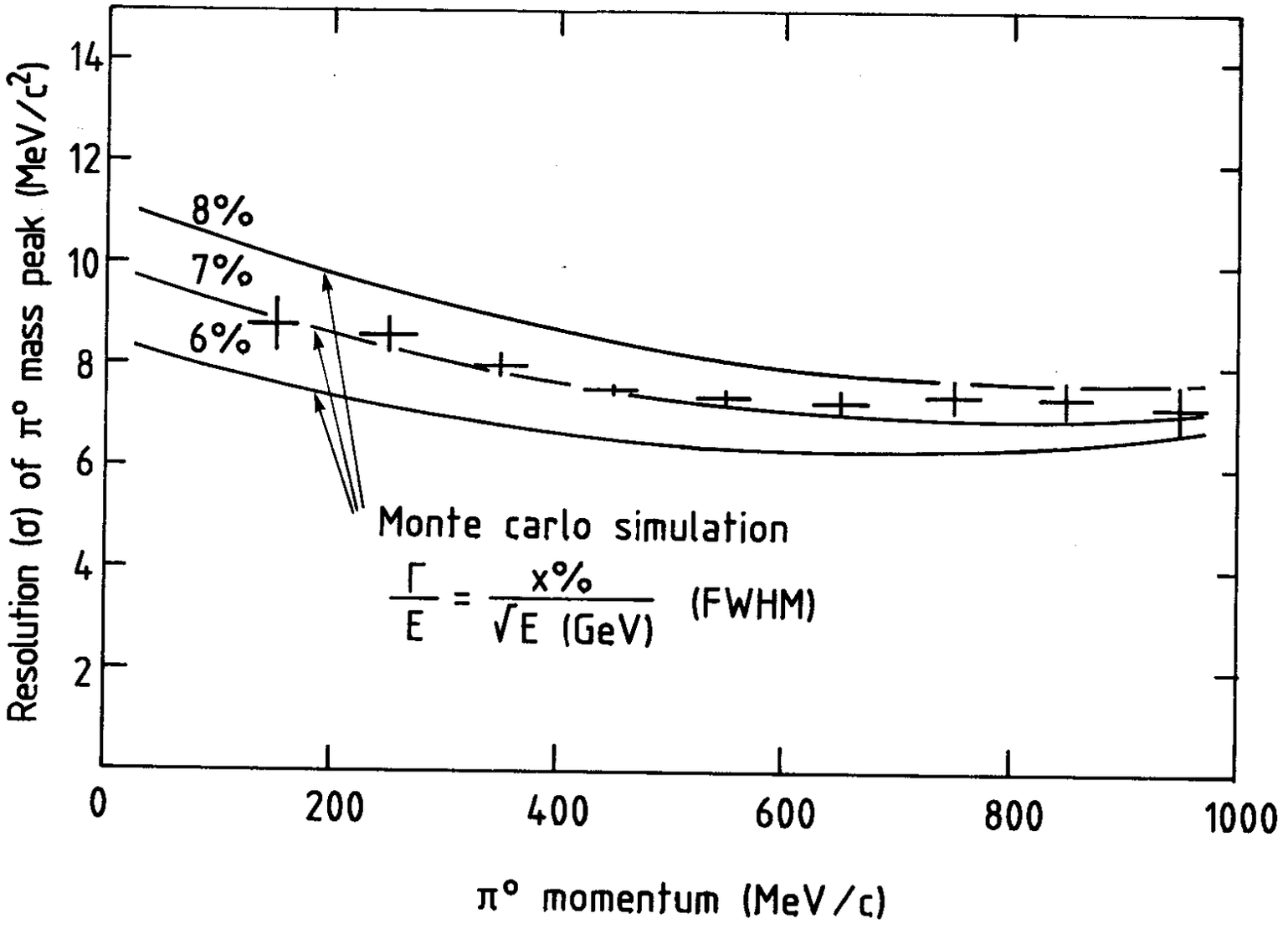
Resolution (σ) of π° mass peak (MeV/c²)
14
12
10
8
6
4
2
8%
7%
6%
Monte carlo simulation
Γ/E = x%/√E (GeV) (FWHM)
0
200
400
600
800
1000
π° momentum (MeV/c)

Fig. 12

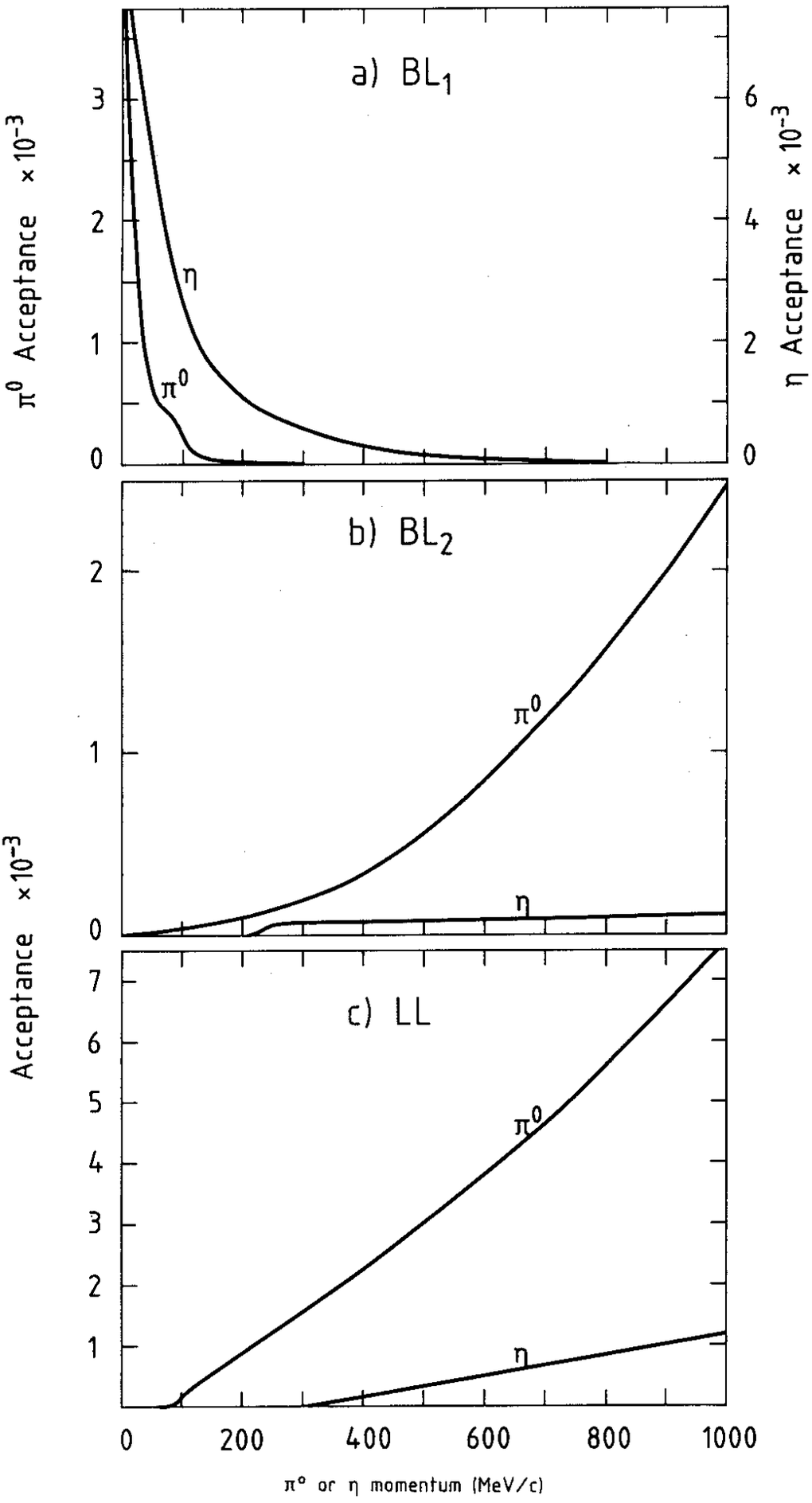
a) BL1
b) BL2
c) LL
π0 Acceptance ×10-3
η Acceptance ×10-3
Acceptance ×10-3
π0
η
0
200
400
600
800
1000
π° or η momentum (MeV/c)

Fig. 13

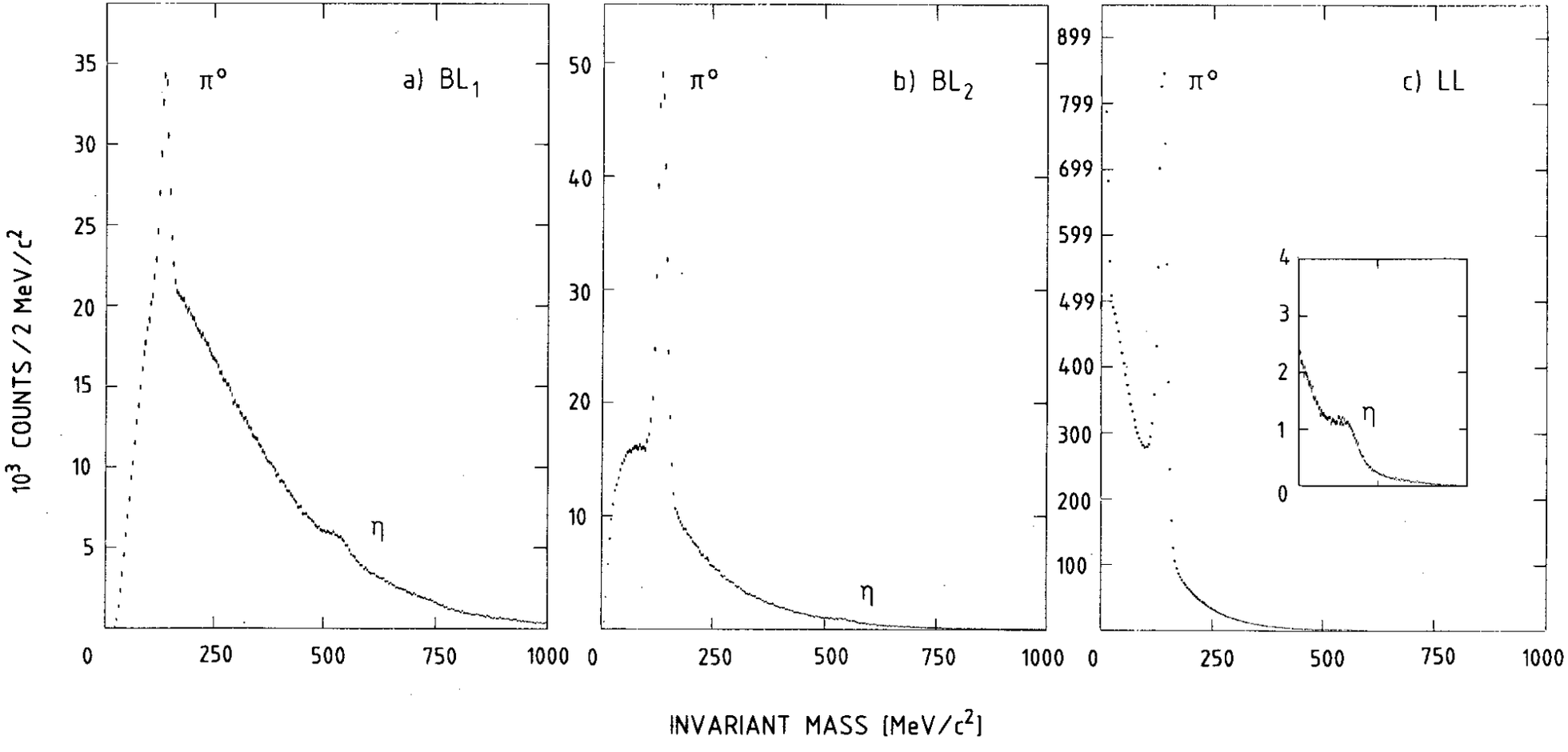

Fig. 14

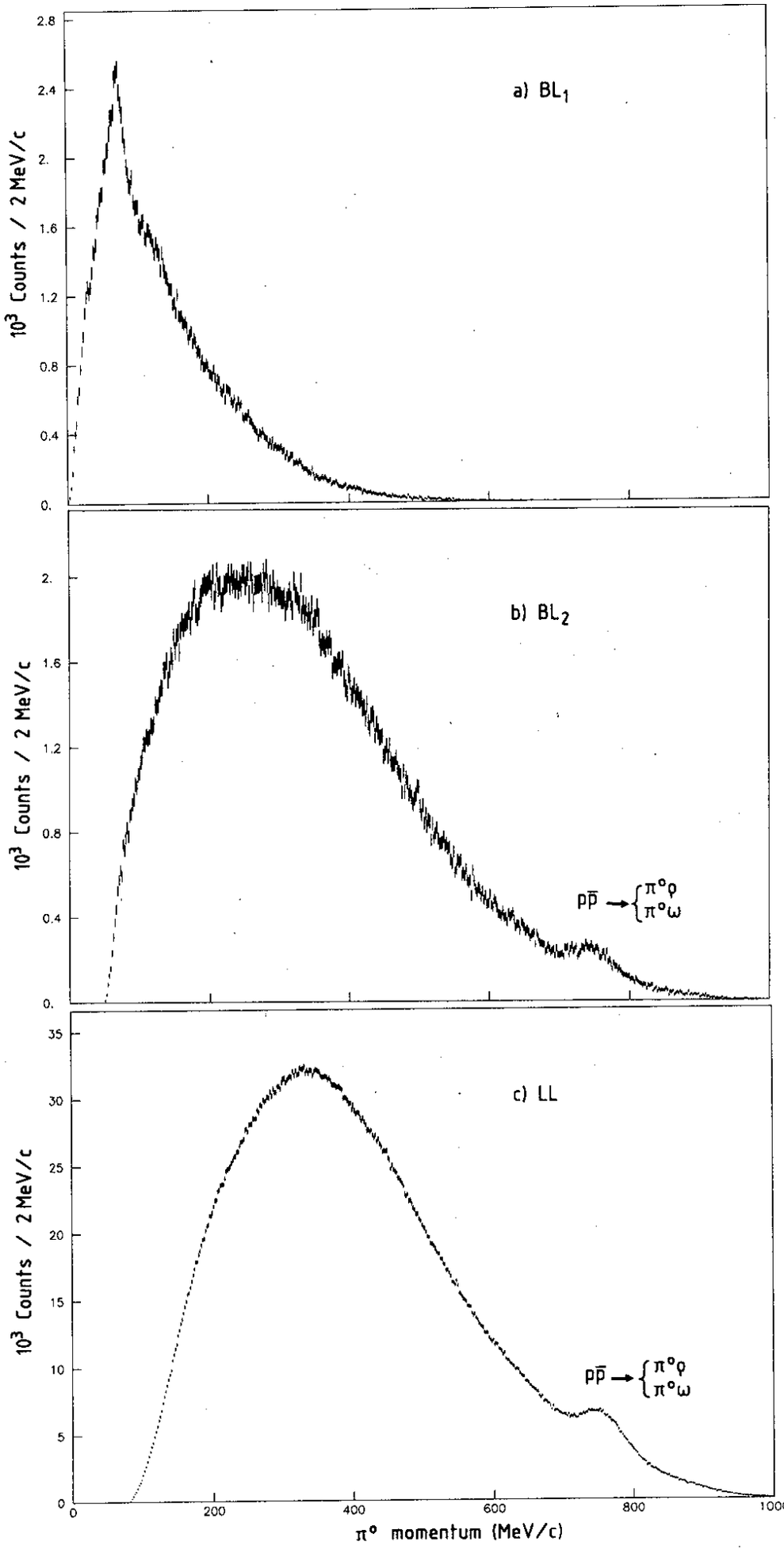
a) BL1
b) BL2
c) LL
$p\bar{p} \rightarrow \{\pi^0\rho, \pi^0\omega$
10^3 Counts / 2 MeV/c
π° momentum (MeV/c)
0
200
400
600
800
1000

Fig. 15

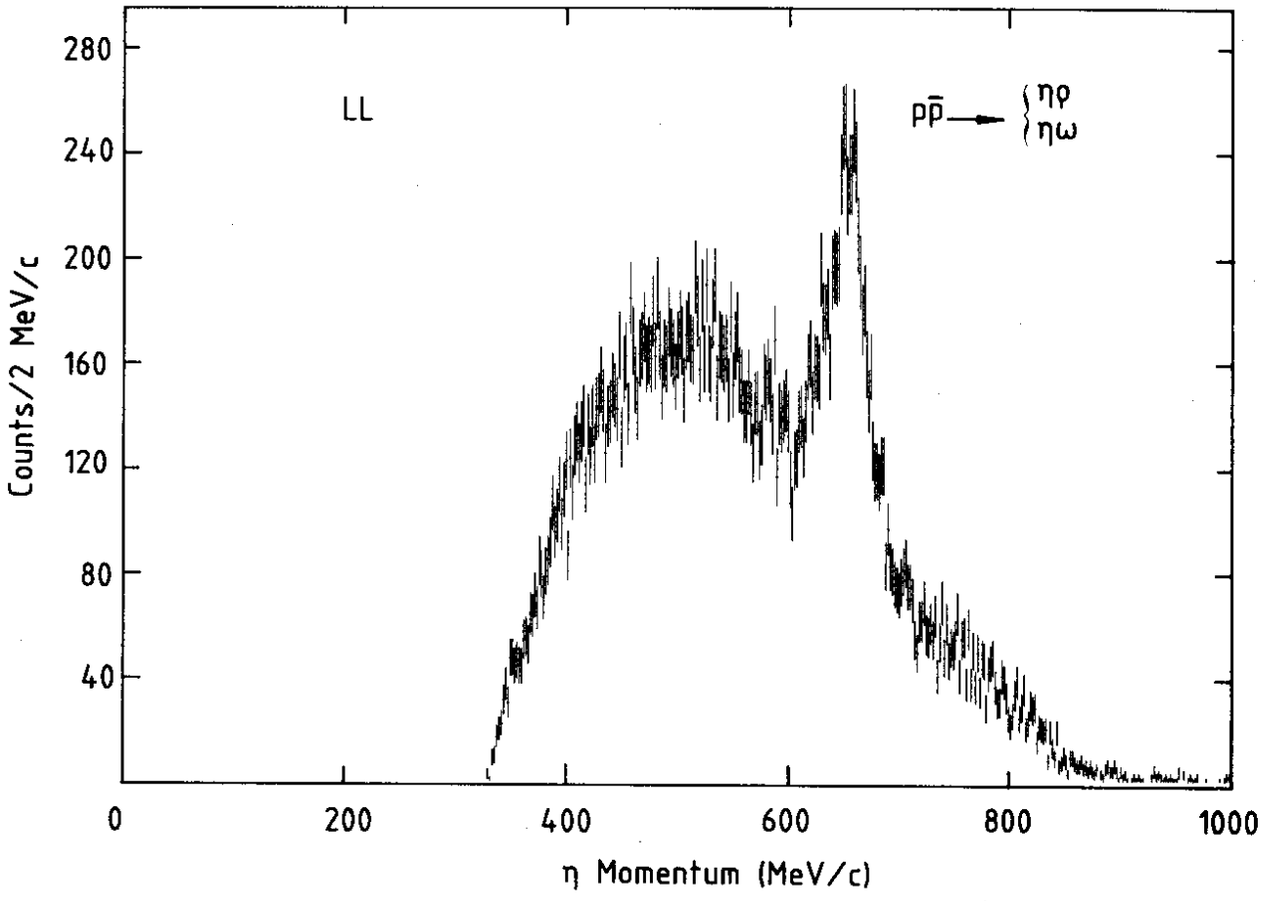
LL
$p\bar{p} \rightarrow \begin{cases} \eta\rho \\ \eta\omega \end{cases}$
Counts/2 MeV/c
280
240
200
160
120
80
40
0
200
400
600
800
1000
η Momentum (MeV/c)

Fig. 16

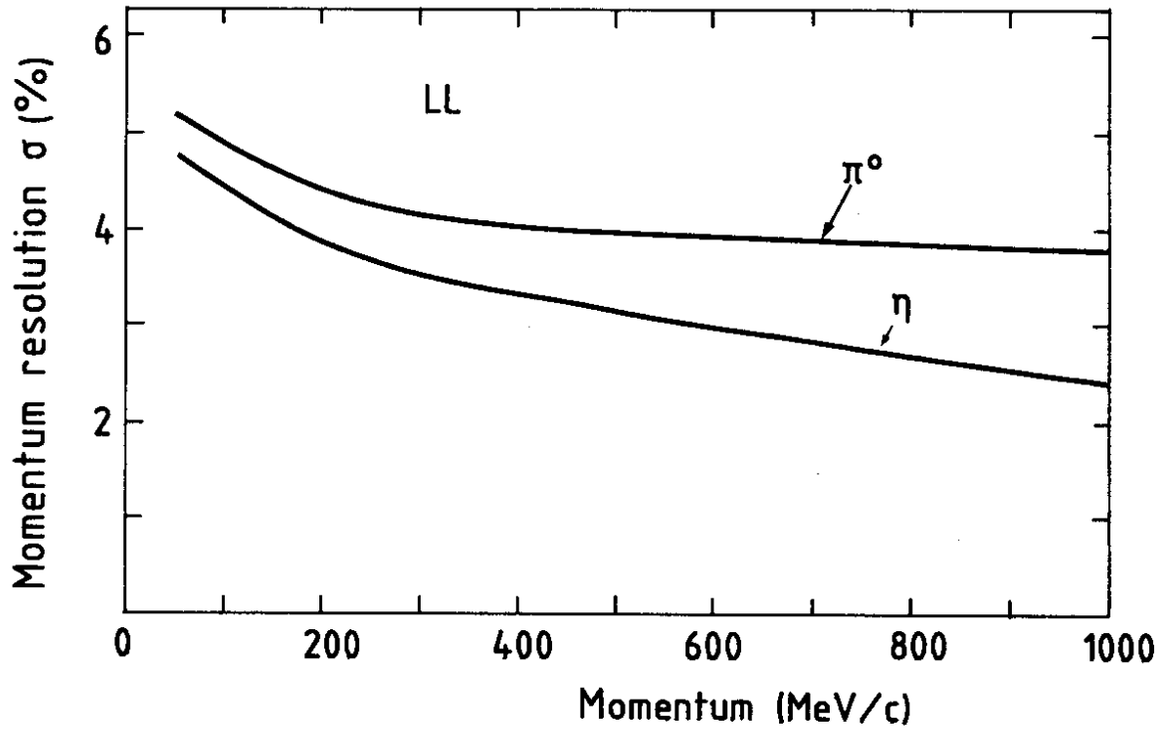
LL
π°
η
Momentum resolution σ (%)
6
4
2
0
200
400
600
800
1000
Momentum (MeV/c)

Fig. 17